Bull. Chem. Soc. Jpn., 72, 1013—1023 (1999)

How to Evaluate the Structure of a Tetranuclear Mn Cluster from Magnetic and EXAFS Data: Case of the S_2-State Mn-Cluster in Photosystem II

Koji Hasegawa, Taka-aki Ono, Yorinao Inoue,† and Masami Kusunoki*,††

Photo-biology Team, Photodynamics Research Center, The Institute of Chemical and Physical Research (RIKEN), Aoba, Sendai, Miyagi 980-0869

†Photosynthesis Research Laboratory, RIKEN, Wako, Saitama 351-0198

††Department of Physics, School of Science and Technology, Meiji University, Tama, Kawasaki, Kanagawa 214-8571

(Received November 24, 1998)

A theoretical method to extract structural information on spin-exchange-coupled manganese tetramers from the EPR spectroscopy data is presented. This method has been applied to two EPR data, i.e. the ground-state spin ($S = 1/2$) and the first excitation energy (30—37 cm^{-1}), for the S_2-state Mn tetramer in the photosynthetic oxygen-evolving complex, which exhibits a "$g = 2$ multiline" EPR signal. Based on the EXAFS data and the manganese chemistry, a simplified model spin Hamiltonian to describe the S_2-state Mn cluster will be presented, such that two spin-exchange interactions due to 2.7—2.8 Å and/or 3.2—3.5 Å Mn–Mn bonds can vary from weak to strong coupling, sensitively, depending upon the bridge structure, except for a strong-antiferromagnetic interaction due to a 2.7 Å Mn(III)–Mn(IV) bond and the other weak ones. By computer-search of the possible spin-exchange structures with respect to these two parametric interactions, it was found that (1) a dimer of di-μ_2-oxo bridged Mn dimers, a propeller-type tetramer in which the central Mn ion is chelated by three di-μ-oxo Mn cores and some other models are highly unlikely, (2) the most promising cluster is a trimer-plus-monomer type of distorted cubane, and (3) $S^* = 5/2$ excited states are higher than the first excited state with $S^* = 3/2$ (majority) or $S^* = 1/2$ (minority).

Photosynthetic water cleavage is carried out by an oxygen-evolving complex (OEC) present on the donor side of photosystem (PS) II. It is believed that a tetranuclear Mn cluster located at the lumenal side of PSII protein complexes accumulates positive charges and provides a catalytic site for water oxidation.[1—4] The reaction process involves five intermediate states, labeled S_i ($i = 0$—4), in which S_1 is thermally stable in the dark.[5,6] In the dark-adapted PSII, the S_1 state advances stepwise by absorbing successive photons to the highest oxidation S_4 state, which then spontaneously decays to the S_0 state with a concurrent release of molecular oxygen. X-Ray absorption near-edge structure (XANES) studies have indicated that the S-state transitions involve a change in the oxidation state of the Mn-cluster.[7—10] The structure of the Mn-cluster and the mechanism of water oxidation are still largely unknown in spite of numerous efforts.

Since a manganese ion has both electronic and nuclear spins, EPR spectroscopy has been applied extensively to the Mn-cluster in order to obtain information regarding its magnetic and structural characteristics. Among the S states, S_2 is the first intermediate state which could be detected by an EPR signal characteristic to the Mn-cluster, called a "multiline" signal, at low temperatures (see for reviews[11,12]). The multiline signal at X-band frequency is centered at $g = 2$ with a spectral width of approximately 180 mT, and exhibits 18—20 partially resolved hyperfine lines.[13] Simulations of the spectrum lead to different conclusions that an $S = 1/2$ Mn-cluster responsible for the signal would be a Mn(III, IV) dimer,[13,14] a Mn(III,IV,III,III) tetramer,[15,16] or Mn(III, IV,IV,IV) tetramer.[17,18] From a Curie-law type temperature dependency observed for the signal intensity, it has been concluded that the signal arises from the ground state.[19—21] The first excited -state spin manifold was determined to lie approximately 35 cm^{-1} above the ground state, utilizing the fact that signal relaxation takes place via the Orbach process through the excited state.[19—21] The discovery of the signal provided evidence that manganese ions form a multinuclear cluster including an antiferromagnetically coupled Mn(III)-Mn(IV).[14—17,22,23] Especially, the fact that the multiline signal is dramatically modified by either Ca^{2+}-depletion or a NH_3-treatment[1] has been ascribed to the sensitivity of the tetrameric spin wave function to a conformational change of the Mn cluster.[17]

EXAFS studies of the normal Mn-cluster indicated the presence of the two kinds of distances between manganese ions, 2.7 and 3.3 Å, and the presence of O(N) ligands at around 1.8 and 2.0—2.1 Å.[24—29] The results have been interpreted as implying that di-μ_2-oxo bridged and mono-μ_2-oxo bridged Mn–Mn subunits with bond distances of 2.7 and 3.3 Å, respectively, are involved. Many structural models

for the Mn-cluster have been proposed based on this finding, although the information from the EXAFS data alone is too limitedto draw a conclusive picture.

Any model proposed for this S_2-state Mn-cluster must be able to explain the observed magnetic properties of the $g = 2$ multiline signal. However, only a few studies that attempt to explain the magnetic properties of the cluster have been reported, because of the molecular structure being unknown and the eigenvalue problem being very complicated in the general case. Hitherto, the spin-exchange problem in a tetranuclear Mn-cluster was challenged by assuming some specific magnetic structures.[13,15—17,24] For instance, a system of a Mn(III,III) dimer exchange-coupled to a Mn(III,IV) dimer with C_{2D}-symmetry as for exchange coupling constants between them was solved using the conventional vector-coupling rules.[13] In a more generalized Mn tetramer containing only one strong-antiferromagnetically coupled Mn(III)–Mn(IV) dimeric subunit, the spin-exchange Schrödinger equation was analytically solved.[17] Moreover, the spin-exchange problem in some specific models of the Mn tetramer was numerically solved by evaluating the matrix elements of the Heisenberg operator, $H_{ex} = \sum_{i<j} J_{ij}\boldsymbol{S}_i\cdot\boldsymbol{S}_j$, for some sets of J-values.[30] However, these studies do not cover all of the possible models for the S_2-state Mn-cluster.

In this paper, we present a comprehensive analytical formulation to calculate observables associated with EPR experiments. In order to demonstrate how to evaluate the structure of a tetranuclear Mn cluster with low symmetry from some EPR data, we have took up the S_2-state Mn cluster in PSII and two EPR data from it, because this cluster has the advantage of being under some structural constraints due to an EXAFS data analysis in conjunction with the accumulated data on the J vs. R relation in binuclear, trinuclear and tetranuclear Mn(III) and/or Mn(IV) compounds. Under this restriction for the Mn cluster, we conducted a computational search for all the possible structures of exchange-couplings between Mn spins (Fig. 1a) as regards whether it satisfies or not the observed energetics data for the S_2-state Mn-cluster responsible for the multiline signal, i.e. (1) $S = 1/2$ ground state, and (2) lowest excited states lying 20—50 cm^{-1} above it, as illustrated in Fig. 1b.

Methods

The Spin-Hamiltonian and Its Eigenstates. The zero-field splitting (ZFS) term for the Mn-cluster may be assumed to be dominated by the Jahn–Teller ion, Mn(III), since its value is typically 1—5 cm^{-1} in magnitude,[31—34] while that is much smaller in Mn(IV) (by two orders of magnitude) than in Mn(III).[35] The ZFS term is not involved in the energy level of the $S = 1/2$ ground state, but can introduce an unnegligible anisotropic excitation energy into an $S > 1/2$ excited state. Therefore, the ZFS effect of order $\pm$ 5 cm^{-1} must be involved in an orientation-dependent excitation energy (see below), although the Zeeman term (0.15—0.41 cm^{-1} in X-band EPR) and the hyperfine interaction terms ((6.8—8.5)$\times 10^{-3}$ cm^{-1} for Mn(III) and Mn(IV) ions) can be safely neglected.

The energy difference between the first excited state and ground-state spin manifolds of the normal Mn-cluster have been found to be 30 cm^{-1} [20] and 31 cm^{-1},[19] and 36.5 cm^{-1} [21] by measuring

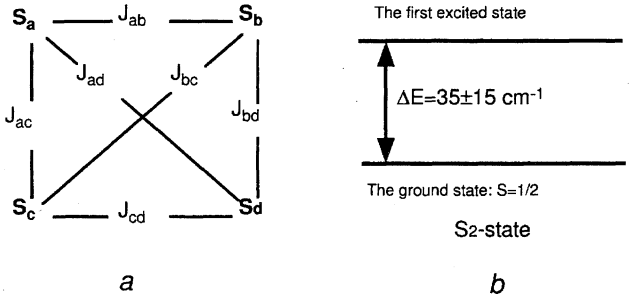

Fig. 1. (a) The exchange coupled four-spin system: $\boldsymbol{S}_i$ represents the i-th spin and $J_{ij}\,\boldsymbol{S}_i\cdot\boldsymbol{S}_j$ the spin-exchange interaction. (b) The S_2-state Mn cluster responsible for "multiline" EPR signal has the $S = 1/2$ ground state and the first excited state(s) at energy ΔE as indicated.

the electron spin-lattice relaxation rate ($1/T_1$) of the multiline signal in CW and Pulsed-EPR spectroscopies, respectively. The value obtained by a Pulse experiment may be more reliable than by a CW experiment, because Pulsed-EPR spectroscopy can directly measure the electron spin-lattice relaxation rate, though it may somewhat depend on the sample preparation. It is of note that the energy difference is an average over all directions, so that the anisotropic ZFS effect on it may be negligibly small. Moreover, all of the known di-μ_2-oxo and mono-μ_2-oxo bridged Mn(III)–Mn(IV) compounds have been found to have the $S = 1/2$ ground state, indicating that the double-exchange mechanism is not explicitly working in these molecular systems. All of the EPR signals due to various S-states are compatible with a picture of localized valence d-electrons in the Mn cluster. Under these conditions, the energy levels of the ground and excited spin states of the Mn-cluster can be determined by considering the spin-exchange Hamiltonian alone, $H_{ex} = \sum_{i<j} J_{ij}\boldsymbol{S}_i\cdot\boldsymbol{S}_j$, where $\boldsymbol{S}_i$ is the i-th spin operator (i = a,b,c,d), taking with the magnitude of 2 and 3/2 for Mn(III) and Mn(IV) ions, respectively, owing to Hund's rule.

Spin Levels of Tetranuclear Clusters. In general, since H_{ex} commutes with the z-component (S_z) of the total spin operator, $\boldsymbol{S} = \sum_i \boldsymbol{S}_i$, and $\boldsymbol{S}^2$, the eigenstate for H_{ex} can be labeled by a set of quantum numbers, (S, M, n), where S is the total spin of the system, M is the azimuthal quantum number, and n is the numbering for different eigenstates belonging the same total spin (S). Therefore, the eigenvector-eigenvalue problem is simply to solve a group of Schrödinger equations;

$$H_{ex} \mid \Phi_{nSM} > = E_{nS} \mid \Phi_{nSM} >, \qquad (1)$$

where S decreases by 1 from the maximum value, $S_a+S_b+S_c+S_d$, until 0 or 1/2, M takes $2S+1$ integer or half-integer values from $-S$ through S. In the S_2-state Mn-cluster, the minimum value of S is 1/2. For the maximum S, there is only one state ($n = 1$), but for $S = 1/2$ there are 7 eigenstates for the Mn(III,IV,IV,IV) and 8 eigenstates for Mn(III,IV,III,III) cluster. The total number of eigenstates must be equal to $\prod_i (2S_i+1)$.

The coupling of $\boldsymbol{S}_i$ and $\boldsymbol{S}_j$ to give a total spin state, (S_{ij}, M_{ij}), is uniquely determined by

$$|S_{ij}M_{ij}> = \sum_{M_i,M_j} C^{S_{ij}M_{ij}}_{S_iM_iS_jM_j} |S_iM_i> \otimes |S_jM_j>$$

with the Clebsch–Gordan coefficient $C^{S_{ij}M_{ij}}_{S_iM_iS_jM_j}$,[36] where $\otimes$ stands for the direct product. This coupling rule must be repeatedly applied

to obtain the total spin states (S, M) for tetranuclear spins. There are in general 15 ways for different coupling schemes. In the S_2-state Mn-cluster, however, S_a and S_b could be assigned to the Mn(III) and Mn(IV) ions, respectively. Hence, the order of couplings is simply branched into two different coupling schemes, "serial" and "pairwise", yielding the following state vectors:

$$|S_aS_b(S_{ab})S_c(S_{abc})S_dSM> = \sum_{m_i,m_{ij},m_{ijk}} C^{SM}_{S_{abc}M_{abc}S_dM_d} C^{S_{ab}M_{ab}}_{S_aM_aS_bM_b} C^{S_{abc}M_{abc}}_{S_{ab}M_{ab}S_cM_c} \times |S_aM_a> \otimes |S_bM_b> \otimes |S_cM_c> \otimes |S_dM_d> \quad (2a)$$

$$|S_aS_b(S_{ab})S_cS_d(S_{cd})SM> = \sum_{m_i,m_{ij}} C^{SM}_{S_{ab}M_{ab}S_{cd}M_{cd}} C^{S_{ab}M_{ab}}_{S_aM_aS_bM_b} C^{S_{cd}M_{cd}}_{S_cM_cS_dM_d} \times |S_aM_a> \otimes |S_bM_b> \otimes |S_cM_c> \otimes |S_dM_d>, \quad (2b)$$

where S_{ab}, S_{cd}, and S_{abc} are the intermediate spins., taking the values, $|S_i - S_j|, \cdots, S_i + S_j$ (i, j = a, b; c, d; ab, c). In terms of these state vectors, the eigenstate vector $|\Phi_{SMn}>$ for the Mn cluster can be expanded as

$$|\Phi_{nSM}> = \sum_{S_{ab},S_{abc}} C_n(S_{ab},S_{abc},S,M) |S_aS_b(S_{ab})S_c(S_{abc})S_dSM> \quad (3a)$$

or

$$|\Phi_{nSM}> = \sum_{S_{ab},S_{cd}} C_n(S_{ab},S_{cd},S,M) |S_aS_b(S_{ab})S_cS_d(S_{cd})SM> . \quad (3b)$$

In Appendix, we have presented analytical expressions for the general matrix elements of H_{ex} between the spin state vectors defined by Eqs. 2a and 2b, which can be derived by applying the Wigner–Eckart theorem and some formulae involving tabulated Wigner 6-j symbol coefficients.[37—39] We remark here that the reported matrix elements[30,39] have been corrected and/or generalized in this paper.

Experimental Constraints for the S_2-State Mn Cluster. EXAFS studies on normal PSII membranes revealed the presence of at least one short (ca. 2.7 Å) Mn–Mn bond in the S_2-state Mn cluster[27,28] which can exhibit the $g = 2$ multiline and/or $g = 4.1$ EPR signal. This sharp Mn–Mn peak was found to split into at least two shells upon a NH_3-treatment, indicative of the ammonia binding being able to lift its degeneracy into ca. 2.7 Å and ca. 2.87 Å Mn–Mn bonds.[40] In Fig. 2, we have collected the reported data of the J vs. R relation for authentic polynuclear Mn(III), Mn(III)/Mn(IV) and Mn(IV) compounds.[41—48] As can be seen from Fig. 2, the Mn–Mn bond elongated up to 2.87 Å can most likely be weak-antiferromagnetic. Nevertheless, the NH_3-treated S_2-state shows only a slight modification of the multiline and $g = 4.1$ signals.[48] These observations can be reasonably explained by assigning an invariant "2.7 Å" bond to a strong-antiferromagnetic Mn(III)–Mn(IV) interaction. Together with an unified point of view, as for a variety of EPR signals in the S_1- and S_2-states, one may assume the existence of this Mn_a(III)–Mn_b(IV) core in the S_2-state Mn cluster. The spin-exchange interactions between 2.64—2.75 Å distant Mn(III)–Mn(IV) ions in authentic Mn complexes were found to be in the range 237—318 cm^{-1} for 2.734—2.643 Å di-μ_2-oxo[45,47] and 228 cm^{-1} for 2.668 Å di-μ_2-oxo-μ_2-carboxylato bridge.[42] Therefore, this subunit may be assumed to have a typical strong-antiferromagnetic spin-exchange interaction, J_{ab} = 250 cm^{-1}, throughout this paper.

On the other hand, a number of di-μ_2-oxo bridged Mn(IV)–Mn(IV) dimers have been reported to take somewhat more widely distributed strong-antiferromagnetic exchange interactions, J = 168—352.9 cm^{-1}, in a similar range of R = 2.672—2.748 Å,[46,47,50] while, surprisingly, only one di-μ_2-oxo bridged Mn(III)–Mn(III) dimer has been reported to take 172 cm^{-1} with R = 2.676 Å.[47] Notably, however, the di-μ_2-oxo bridged Mn(IV)–Mn(IV) interaction tends to be significantly intensified (248—440 cm^{-1}) and significantly shortened (2.58—2.588 Å) by coordination of a third μ_2-carboxylato bridge,[47] but in the presence of the μ_2-O_2Mn bridge to be slightly weakened (152—182 cm^{-1}) and shortened (2.565—2.681 Å). Taking these "di-μ_2-oxo" bridged manganese dimers into account, one can define a group of strong-antiferromagnetic interactions with 168 $cm^{-1} \leq J_{ij} \leq 300$ cm^{-1} in the range 2.65—2.75 Å (see Fig. 2). The strong-antiferromagnetic "2.7 Å" Mn(III/IV)–Mn(III/IV) bond in OEC can be designed by not only the simplest di-μ_2-oxo bridge, but also more sophisticated μ_2-oxo-μ_3-oxo, μ_2-oxo-μ_3-oxo-μ_2-carboxylato, μ_2-oxo-μ_3-oxo-μ_2-OMnO, and μ_2-oxo-μ_3-oxo-μ_2-(aqua,hydroxo) bridges, as depicted in Scheme 1. The possible

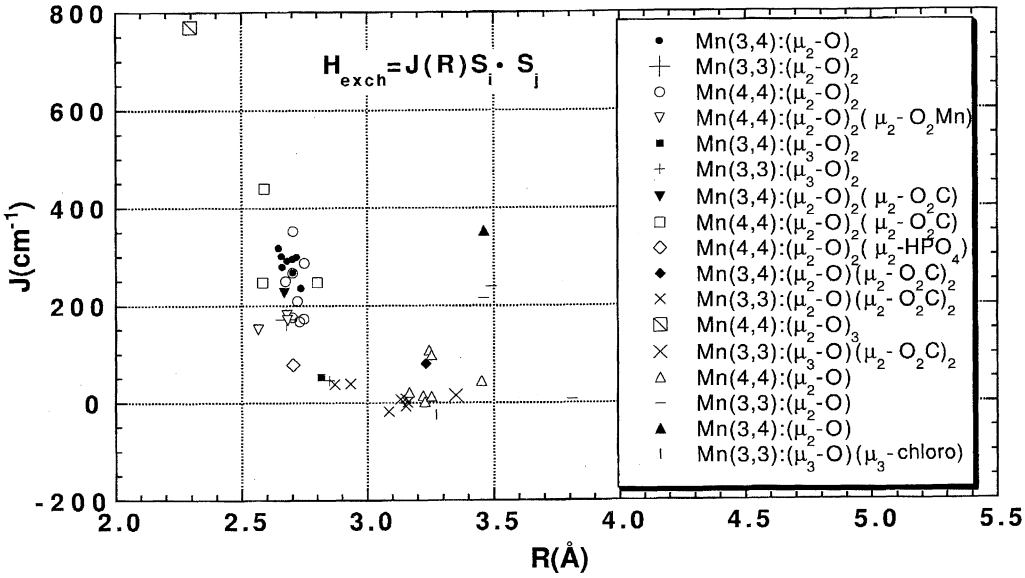

Fig. 2. The spin-exchange interactions between high-valent manganese ions, i.e. Mn(III)–Mn(III) (+, −, |, ×), Mn(III)–Mn(IV) (full marks), and Mn(IV)–Mn(IV) (open marks), plotted as a function of the Mn–Mn distance (R) and the bridging ligand(s), which are minimally described in inset.

existence of a μ_2-(aqua,hydroxo) bridge was demonstrated in diiron-(III) complexes.[51] An exceptional case is an inorganic phosphate bridge between di-μ_2-oxo bridged Mn(IV)–Mn(IV) ions, which is reported to drastically weaken the J-value into 79 cm^{-1} at $R = 2.701$ Å (but, this would be irrelevant to OEC),[52] although it might be taken into account as a weak-to-strong coupling parameter.

As R increases from 2.75 to 2.8 Å, the J-value dramatically drops down to weak-coupling (see Fig. 2). This behavior can be well understood as a cancellation effect, such that the antiferromagnetic stabilization energy due to the formation of a direct $d\gamma$–$d\gamma$ bond between Mn–Mn ions, which exponentially decays as R increases, would balance with the ferromagnetic superexchange energy through di-μ_2-oxo bridges around this region (as predicted by the second Goodenough–Kanamori rule). Notably, this empirical relation or rule would hold for both μ_2-oxo and μ_3-oxo bridges between Mn(III)/Mn(IV) ions.

In particular, a bridge group involving the μ_3-oxo unit can also become likely candidates for the other short Mn–Mn bond(s) in the cluster, which may be allowed by EXAFS studies to assume that the number is less than 2 and the bond length might range from 2.65 to 2.80 Å. Therefore, this bond must be treated as parameter(s) that can change from weak- to strong-antiferromagnetic coupling.

Another interesting bridge is associated with the "3.3 Å" Mn–Mn bond observed as the third peak in the EXAFS Fourier transform.[30,25,28,29] Possible candidates for the bridge ligands in the Mn cluster would be μ_2-oxo-di-μ_2-carboxylato, μ_3-oxo-di-μ_2-carboxylato, μ_2-oxo, μ_3-oxo, μ_2-oxo-μ_2-carboxylato, μ_3-oxo-μ_2-carboxylato, μ_3-oxo-μ_3-chloro, and so on, as illustrated in Scheme 2. Among them, a μ_2-oxo bridge with a Mn–O–Mn angle ($\theta \approx \pi$) was predicted by the first Goodenough–Kanamori rule to induce an antiferromagnetic superexchange interaction between Mn(III)/Mn(IV) ions via the nearly linear μ_2-oxo bridge, although which can also somewhat depend not only on the relative energy levels between Mn and O orbitals, but also on two Mn–O bond lengths. This prediction is evidenced in Fig. 2 by a μ_2-oxo bridged Mn(III)–Mn(IV) interaction with $J = 353$ cm^{-1} at $R = 3.46$ Å,[48] and μ_2-oxo bridged Mn(III)–Mn(III) interactions with $J = 216$, 240 cm^{-1} at $R \approx 3.46$, 3.49 Å,[50] respectively. However, as θ decreases from π, the J-value appears to rapidly decrease and become intermediate, e.g. $J = 80$ cm^{-1} at $R = 3.23$ Å in μ_2-oxo-di-μ_2-carboxylato Mn(III)–Mn(IV) dimer[43] and $J = 98.0$ cm^{-1}, 108 cm^{-1} at $R = 3.254$ Å, 3.242 Å, respectively, in mono-μ_2-oxo Mn(IV)–Mn(IV) dimers,[47] or even weak, e.g. $J = 45$—2.7 cm^{-1} in the range, $R = 3.166$—3.452 Å, in mono-μ_2-oxo Mn(IV)–Mn(IV) dimers[46] and $J = -18$—8.2 cm^{-1} at $R = 3.084$—3.159 Å in μ_2-oxo-di-μ_2-carboxylato Mn(III)–Mn(III) dimers.[43] Therefore, the J-value through this "3.3 Å" bridge must also be treated as another unknown parameter that is variable from weak- to strong-coupling.

Consequently, it was found that the S_2-state Mn cluster would most probably contain (i) one strong-antiferromagnetic Mn-(III)–Mn(IV) interaction with $J = 230$–330 cm^{-1} and (ii) two unknown spin-exchange interactions through "another 2.7 Å" and "3.3 Å" Mn–Mn bonds, called "parametric interaction", that may be weak, intermediate or strong, so that (iii) the other three exchange interactions may be assumed to be weak over the range, $J = -20$—40 cm^{-1}.

Based on these magnetic properties and the aforementioned structural constraints, (i), (ii), and (iii), we performed computer

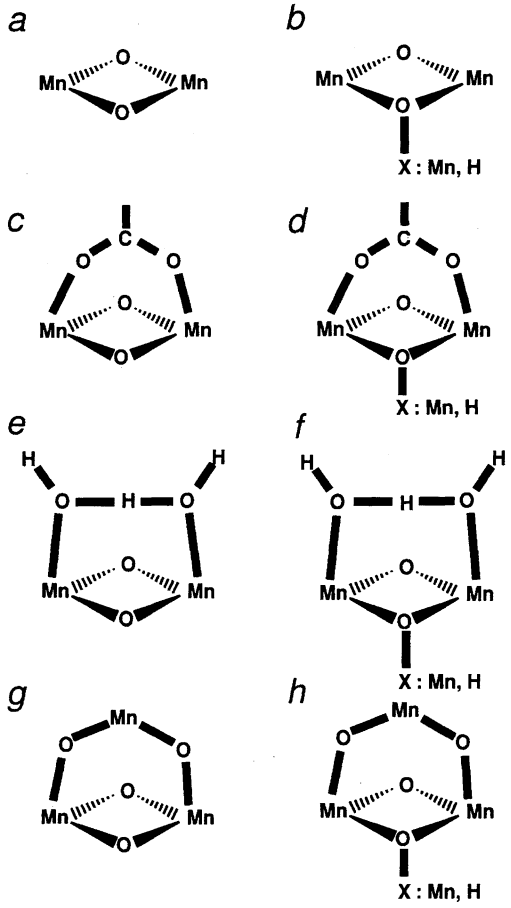

Scheme 1. Likely candidates of bridging ligands responsible for the ca. 2.7 Å Mn–Mn interaction observed in the normal S_1 and S_2 states of OEC.

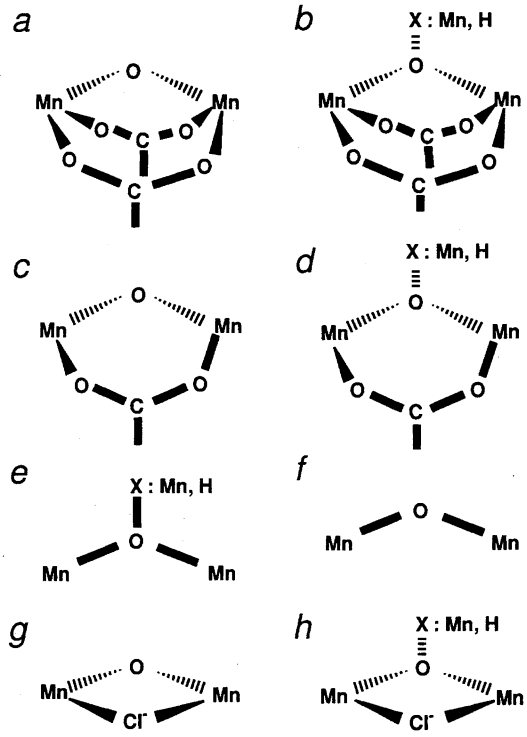

Scheme 2. Likely candidates of bridging ligands responsible for the ca. 3.3 Å Mn–Mn interaction supposed to exist in the normal S_1 and S_2 states of OEC.

experiments to examine all possible model Mn-tetramers in the S_2-state to find out which coupling structures can satisfy the following conditions: (1) the oxidation state of the S_2-state Mn-cluster would be either Mn(III,IV,IV,IV)[9,17,22,27] or Mn(III,IV,III,III);[16] (2) the total spin in the ground state is $S = 1/2$; and (3) the energy difference between the ground-state and the first excited-state spin-manifolds is 35 ± 15 cm^{-1}, which is set so as to involve a rather large uncertainly due to the inhomogeneous broadening, the possible averaging over plural excited-states and a non-averaged-out ZFS contribution, as written in Fig. 1b.

Computer Search. Computations were carried out in both coupling schemes, for a numerical check, with use of our own Fortran program[53] involving calculation of Wigner 6-j symbols according to the Racah formula[37] and numerical diagonalization by the Rutishauser–Jacobi's algorithm.[54] SUN workstations in Meiji University Information and Science Center and a personal computer (PC) equipped with a DEC AXP 433 MHz CPU and 128M byte RAMs were used. A typical run to solve the eigenstate problem for a whole set of spin-exchange interactions (totally, 9282325) for each oxidation state took about 4 h CPU time using the DEC PC.

Results

The valences of the manganese ions in positions a and b may be chosen as Mn(III) and Mn(IV), respectively, in both the Mn(III-IV,IV,IV) and Mn(III-IV,III,III) oxidation states. This strong-antiferromagnetic dimeric subunit is referred to as Mn(III-IV) throughout this paper. Since the Mn-cluster may contain at most two strong-antiferromagnetic interactions in the cluster besides J_{ab}, we have considered ten different magnetic configurations with respect to the two parametric interactions, designated X and Y, chosen from five J_{ij}'s beside J_{ab}. Four among the ten configurations, however, can be eliminated from their symmetric feature for the valence exchange operation of the manganese ions in positions, c and d, which are assumed to be either Mn(IV)–Mn(IV) or Mn(III)–Mn(III) in the S_2 state, which will be referred to as Mn–Mn. The remaining three weak-exchange interactions appoint a position, (x, y, z), in a "weak-coupling cube" in the region, $-20 \leq (x,y,z) \leq 40$. For a given (J_{ab}, X, Y), we can know what positions in the cube do not satisfy the aforementioned magnetic properties of the S_2-state Mn cluster. Such Mn clusters can be eliminated from the candidates for the S_2-state Mn cluster. Oppositely, when the whole cube is occupied by satisfactory points, the (J_{ab}, X, Y)-clusters may be considered to be most likely, because these clusters have the maximum degrees of freedom which can be used to fit into the simulation of the multiline signal. Therefore, as a theoretical index for a structure evaluation, we would use the volume occupancy of satisfactory points in the cube, which may be simply called "probability" at the present level-of-information on the magnetic properties of the S_2-state Mn cluster. This probability is implicitely based on a reasonable assumption that any weak exchange coupling at a protein-active site can take a value in the range -20 cm$^{-1} < J_{ij} < 40$ cm^{-1} with equal probability.

In Fig. 3, we show the results of calculations presented in terms of contour maps of the probability in the respective six configurations for the parametric interactions, (X, Y). The X- and Y-values were independently changed from -20 to 300 cm^{-1} with a 5 cm^{-1} interval and the x, y and z-values from -20 to 40 cm^{-1} with the same interval. The probability is defined by the number ratio of the satisfactory points to the sampling points (which is $13\times13\times13 = 2197$) in the weak-coupling cube, so that the probability is normalized to unity. The $S = 1/2$ ground-state was found to accompany an $S^* = 3/2$ or $S^* = 1/2$ first excited state. No first excited state with higher-spin ($S^* \geq 5/2$) was found. Namely, not only $S^* = 3/2$, but also $S^* = 1/2$, can be responsible for the first excited state spin in the S_2-state Mn-cluster. Since a change of the J_{ab} values in the range 200—300 cm^{-1} did not show any visible effect on the probability distribution, we present only those for $J_{ab} = 250$ cm^{-1} throughout this paper.

In Figs. 3A and 3B, we show the resultant six contour maps where the first excited state has a spin $S^* = 3/2$ in the Mn(III-IV,IV,IV) cluster (A) and the Mn(III-IV,III,III) cluster (B), respectively. The shadowed regions in the map implies that the probability is more than 1/2197. Hence, the magnetic structures corresponding to the non-shadowed region can be excluded from the candidate for the S_2-state Mn-cluster.

Map *a* in Fig. 3A shows the probability distribution for the (J_{ab}, J_{ac}, J_{ad})-type tetramer, which is symmetric for an exchange between J_{ac} and J_{ad}. A somewhat similar map was obtained for the (J_{ab}, J_{bc}, J_{bd})-type tetramer (map *e*), which is valence-exchanged between the a and b sites. These results indicate that the Mn clusters with three strong-antiferromagnetic interactions forming a propeller-type tetramer can be ruled out from the candidates. Furthermore, the most probable structures may contain four weak interactions other than the strong J_{ab} and its neighbor (one of J_{ac}, J_{ad}, J_{bc}, and J_{bd}), which is allowed to vary from weak to strong interactions. Of note is that the effect of a valence exchange between maps, *a* and *e*, appears to be small, but adequate for causing significant signal modulation.

In map *b* in Fig. 3A for the (J_{ab}, J_{ac}, J_{bc})-type tetramer, the non-shadowed region is limited to a narrow upper-right corner, indicating that the Mn clusters with a triangular core formation of 2.7, 2.7—2.87 and 3.3 Å Mn–Mn bonds are most flexible for explaining EPR data, and hence promising. Also, in map *c* for the (J_{ab}, J_{ac}, J_{bd})-type tetramer, the non-shadowed region is observed only in the upper-right corner, although its area is larger than that of map *b* for Mn(III-IV,IV, IV), but smaller for Mn(III-IV,III,III), indicating that the Mn clusters containing an open arrangement of the central 2.7 Å Mn(III)–Mn(IV) bond connected by 2.7—2.87 and 3.3 Å Mn–Mn neighboring bonds would also be acceptable, except for the corner region of $(J_{ac}-300)^2+(J_{bd}-300)^2 < 200^2$ for Mn(III-IV,IV,IV) and $(J_{ac}-300)^2+(J_{bd}-300)^2 < 120^2$ for Mn(III-IV,III,III).

In Fig. 3A, map *d* for the (J_{ab}, J_{ac}, J_{cd})-type tetramer and map *f* for the (J_{ab}, J_{bd}, J_{cd})-type tetramer are quite different from maps, *a*, *b*, *c*, and *e*, both showing non-shadowed regions in the upper-reach and the bottom-left of the maps. This difference arises from the fact that two parallel dimers of Mn_a(III)–Mn_b(IV) and Mn_c(IV)–Mn_d(IV) are bridged by only one parametric bond (2.75—2.8 or 3.2—3.5 Å) in maps,

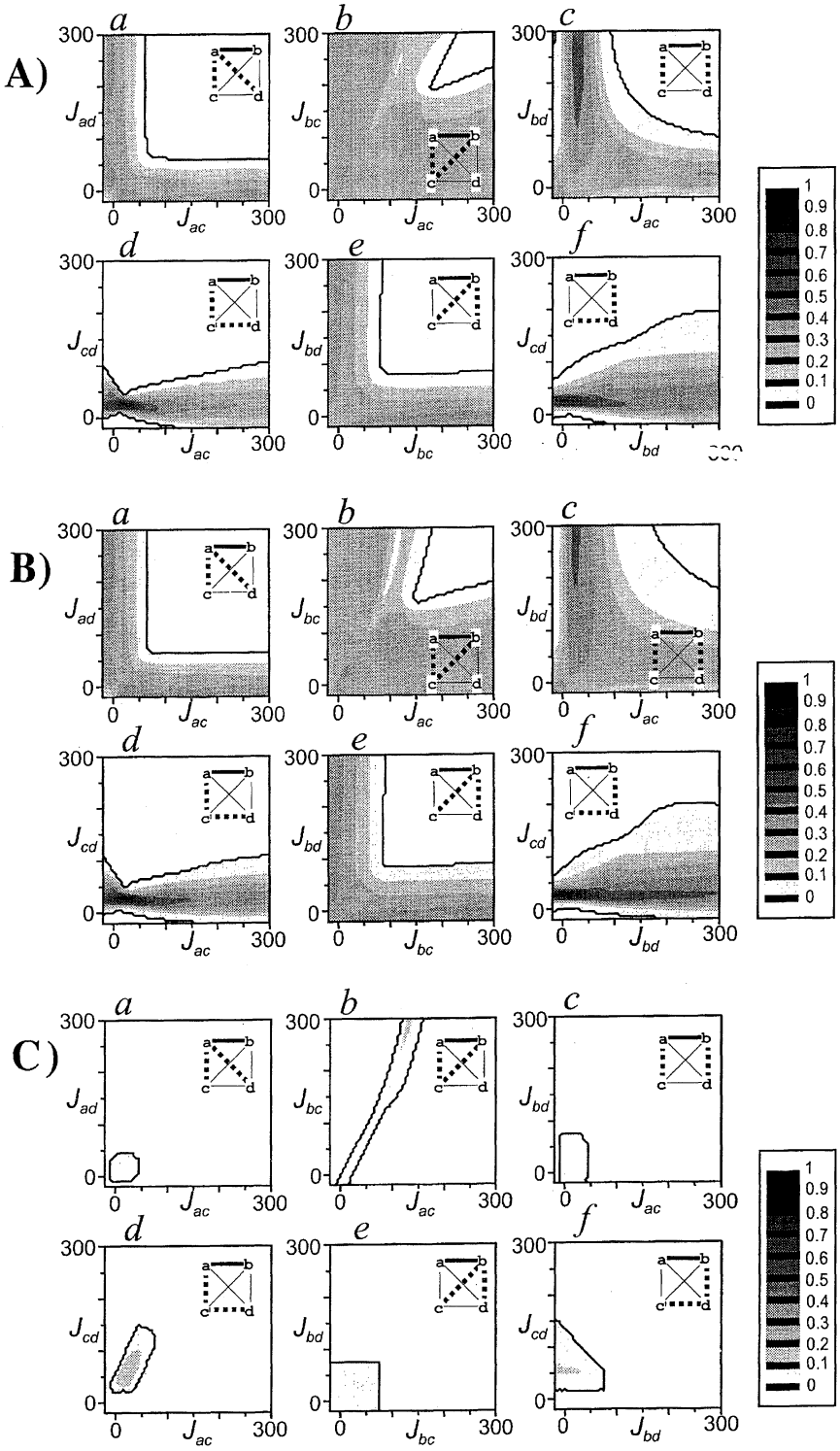

Fig. 3. The probability distributions of a (J_{ab}, X, Y)-type of the S_2-state Mn(III-IV,IV,IV) (A, C) or Mn(III-IV,III,III) (B) tetramer having the $S = 1/2$ ground-state and the first excited state at 20—50 cm^{-1} with each spin $S^* = 3/2$ (A, B) or $S^* = 1/2$ (C). A set of contour maps in six parametric interaction planes (X, Y), representing the volume occupancy of the suitable Mn-clusters with $J_{ab} = 250$ cm^{-1} in the cubic space of three weak-exchange interactions (-20 $cm^{-1} \leq (x,y,z) \leq 40$ cm^{-1}). Thick lines are marked along the boundary at level, 1/2167.

d and *f*, while they are bridged by two parametric bonds (2.75—2.8 and 3.2—3.5 Å) in the others. A remarkable result is that the Mn(III-IV,IV,IV) clusters, whose parallel dimeric subunits are connected by at least three weak-coupling bridges, can be excluded from the candidates unless J_{cd} also becomes weak or intermediate coupling, except for the case of both J_{bd} (> 150 cm^{-1}) and J_{cd} (> 150 cm^{-1}) being strong-antiferromagnetic (see map *f*). This exceptional case

shows a remarkable effect of valence exchange between the a and b sites (a difference between maps, *d* and *f*). Furthermore, the most probable Mn clusters are found to contain only one strong-antiferromagnetic J_{ab} and the other weak interactions.

In the case where the first excited state is in spin $S^* = 3/2$, the characteristic features of the contour maps for the Mn(III-IV,III,III) cluster as shown in Fig. 3B appear to be not significantly different from those for the Mn(III-IV,IV,IV) cluster, as shown in Fig. 3A. Maps *b* and *c* in Fig. 3B are, however, somewhat different from those in Fig. 3A, indicating that the change in the valences (IV→III) of the manganese ions in positions, c and d, can somewhat affect the magnetic properties only in these Mn(J_{ab}, J_{ac}, J_{bc})- and Mn(J_{ab}, J_{ac}, J_{bd})-type tetramers.

Figure 3C shows six contour-maps for the Mn(III-IV,IV,IV) cluster, whose first excited state has a spin $S^* = 1/2$. These maps are considerably different from those for the $S^* = 3/2$ excited-state in Fig. 3A. Notably, the shadowed regions are much narrower and the probability is much smaller in the case of $S^* = 1/2$ than $S^* = 3/2$. This result indicates that the probability for the $S^* = 1/2$ first excited state would be considerably low. The contour maps for the Mn(III-IV,III,III) valence state are almost the same as those for the Mn(III-IV, IV,IV), except for minor differences (data not shown).

Discussions and Conclusions

There is a general consensus concerning the presence of three resolved peaks, designated P_i (i = I, II, III), in the k^n-weighted (n = 2—3) Fourier transforms of the Mn K-edge EXAFS spectra taken from the sample dark-adapted in the normal S_1-state.[24—29] The strong second peak (P_{II}) was well simulated by assuming the presence of about two 2.7 Å Mn–Mn bonds in the cluster. Since such a short 2.7 Å Mn–Mn distance is found from Fig. 2 to be typical to di-μ_2-oxo bridged Mn(III)–Mn(III), Mn(III)–Mn(IV), and Mn(IV)–Mn(IV) complexes, this EXAFS result was taken as strong evidence for the S_1-state Mn cluster to be a dimer of di-μ_2-oxo bridged dimer,[55] which is called the "Berkeley's model". This model is considered to also hold for the S_2-state Mn cluster, which was advanced by 195 K illumination to give rise to the $g = 2$ multiline EPR signal, based on its EXAFS showing very small changes with respect to the S_1-state.[26] Of note is that this model is almost equivalent to assuming the presence of two parallel strong-antiferromagnetic exchange interactions, J_{ab} and J_{cd}, as discussed in the previous section. However, there remains another possibility that the P_{II} peak can be resolved into inequivalent Mn–Mn bonds, even in the normal S_2-state, just as in the NH_3-treated S_2-state where the P_{II} peak split into 2.7 and 2.87 Å Mn–Mn bonds.[40] In fact, it has recently been shown that this peak can be resolved into 2.70 and 2.80 Å Mn–Mn bonds, based on an improved theory of EXAFS data analysis.[56] This implies that the Mn cluster may contain one 2.7 Å Mn(III)–Mn(IV) bond with a strong-antiferromagnetic exchange interaction, and one 2.8 Å Mn–Mn bond with a weak or intermediate interaction (see Fig. 2). This alternative picture of the second peak P_{II} is quite consistent with the fact that the $g = 2$ multiline signal shows only a mild difference between the normal and the NH_3-modified S_2-states. Therefore, we have treated the spin-exchange interaction due to this "2.75—2.8 Å" Mn–Mn bond as the first parametric interaction which can vary from a weak to a strong coupling region. The second parametric interaction was provided by a "3.3 Å" Mn–Mn bond, a possible origin of the third peak P_{III}, because this "3.3 Å" distance between Mn ions has to be quite unreliable and may contain a large uncertainty over the range 3.2—3.5 Å.

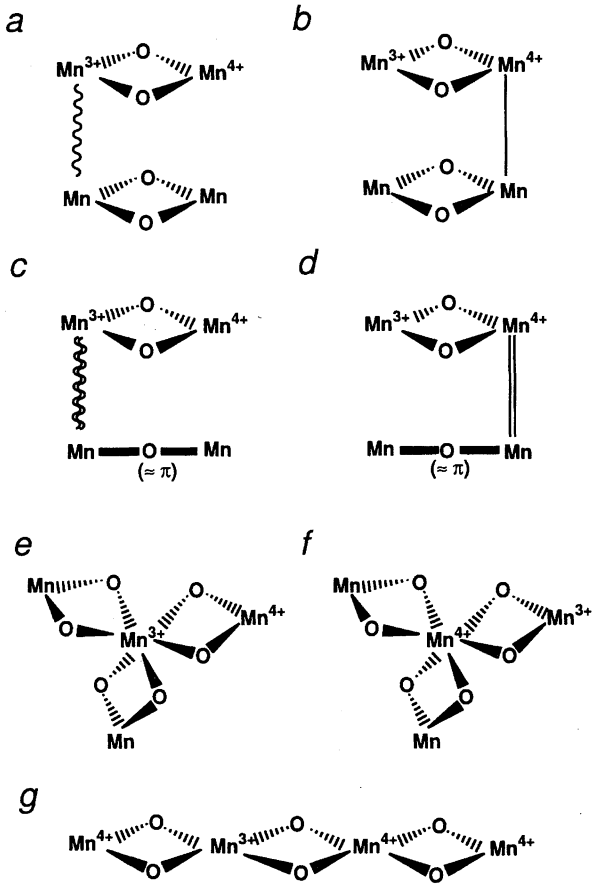

Scheme 3. Model manganese complexes rejectable from likely candidates for the S_2-state Mn cluster in OEC, which can not satisfy the magnetic data: (1) the $S = 1/2$ ground state and (2) the first excited-state lying 20—50 above it, for $J_{ab} > 200$ (in units of cm^{-1}). The absence of line implies $-20 \leq J_{ij} \leq 40$, wave lines $-20 \leq J_{ij} \leq 300$, and solid lines $40 \leq J_{ij} \leq 150$. Single and double lines represent any one of 3.2—3.5 Å bridges in Scheme 2 and 2.75—2.8 Å bridges in Scheme 1, respectively.

To investigate how the S_2-state Mn-cluster is constructed using a 2.7 Å Mn(III)–Mn(IV) bond and not-well-defined 2.75—2.8 Å and 3.2—3.5 Å Mn–Mn bonds, we calculated the probabilities of all types of Mn clusters with respect to the three spin-exchange interactions, (J_{ab}, X, Y), due to these bonds. In all types, a majority of the suitable Mn clusters were found to have the first excited state in spin $S^* = 3/2$ and a minority of them in spin $S^* = 1/2$. No higher spin state (e.g.

$S^* = 5/2$) was found in the first excited states of the suitable Mn clusters with the $S = 1/2$ ground states, indicating that the multiline and $g = 4.1$ EPR signals due to the $S = 1/2$ and $S = 5/2$ S_2-states, respectively, must have arisen from structurally different Mn clusters. This result is consistent with the EXAFS data observed when the OEC is advanced by 130 K illumination to generate the different S_2-state Mn cluster which gives rise to the $g = 4.1$ signal. In this case, one of the short Mn–Mn bonds is elongated to have a larger distance, 2.85 Å,[57] which can induce a dramatic change in the spin-exchange interaction from a weak-antiferromagnetic to a weak-ferromagnetic coupling, as was predicted in an unified interpretation of these S_2-state signals.[23] Furthermore, it was found that these contour maps are remarkably similar between Mn(III-IV,IV,IV) and Mn(III-IV, III,III) oxidation states (Fig. 3A vs.Fig. 3B). This is due to the low spin state.

This probability represents the degrees of freedom given to a set of the remaining three weak exchange interactions which can be used to find the more limited sets of values capable of simulating the multiline signal, although we did not do this in this paper. If this restriction is added to the contour maps, not only the probability (or the volume occupancy) will be dramatically reduced by a factor of order 10^{-2}, but also the non-zero region in the X–Y plane could also be significantly narrowed into such regions of weak or intermediate couplings, in all cases. A preliminary report for this theoretical work has been given.[58] In this work, however, we did not take into account this additional experimental constraint, because it is obliged to tackle additional large ambiguities owing to unknown intrinsic nuclear hyperfine coupling constants ($|a_i| = 70$—90 cm^{-1} for Mn(III) and Mn(IV) ions). Nevertheless, we could distinguish some rejectable model Mn clusters from some acceptable ones, based on the contour maps in Figs. 3A—C.

In Scheme 3, we have illustrated some tetranuclear Mn clusters (skeletal structures only) which can be ruled out from the likely candidates for the S_2-state Mn cluster. The so-called Berkeley's model for the normal S_2-state Mn cluster is involved in *a* and *b*, where the wavy line (in *a*) and the thin solid line (in *b*) may represent any one of the bridge ligands listed in Scheme 2, which is allowed to take the value of spin-exchange interaction in the range, -20 cm$^{-1} \leq J_{ac} \leq 300$ cm^{-1}(a weak-strong coupling) and -20 cm$^{-1} \leq J_{bd} < 150$ cm^{-1} (a weak-intermediate coupling), respectively. Similarly, the Mn clusters belonging to *c* and *d* may be excluded from the likely candidates, where the mono-μ_2-oxo bridged Mn–Mn bond is assumed to take a strong-antiferromagnetic J_{cd} with a bridge angle of ca. π, and a double-wavy line (in *c*) and a double-solid line (in *d*) may represent any one of the bridge ligands listed in Scheme 1, which are allowed to take the J_{ac} and J_{bd} values in the same regions, as mentioned above. Apart from the EXAFS data, we have added to the rejectable model list, propeller-type tetramers in which the central Mn ion is chelated by three di-μ_2-oxo bridged Mn cores (*e* and *f*) and chain-type tetramers in which three di-μ_2-oxo bridges are linearly arranged (*g*). These tetramers may also be rejected for another reason that they are difficult to incorporate a 3.2—3.5 Å Mn–Mn bond in the cluster and, hence, would be inconsistent with the EXAFS data.

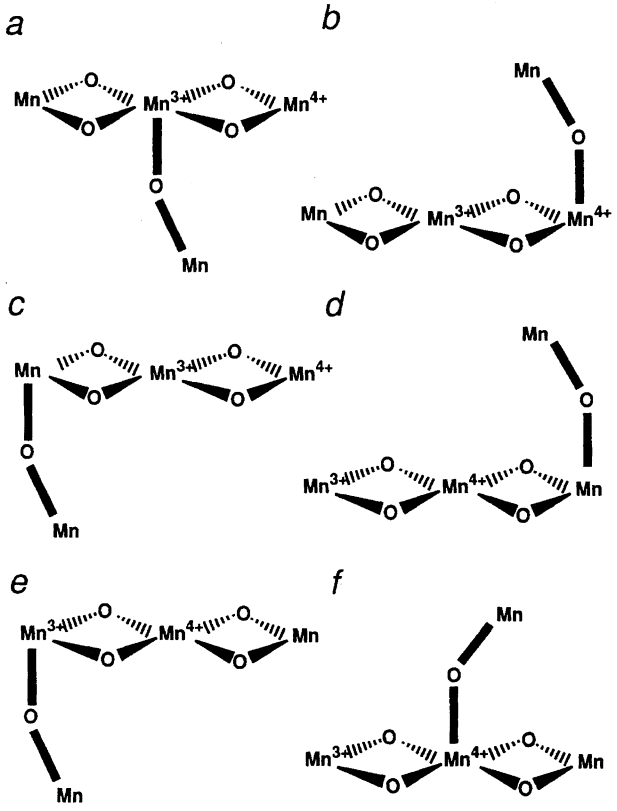

Scheme 4. Acceptable Mn clusters which involve two strong-antiferromagnetic di-μ_2-oxo bridged Mn–Mn interactions (2.7 Å) and a possibly weak-coupling μ_2-oxo bridged one (3.3 Å, bented).

On the other hand, acceptable Mn clusters which involve two strong-antiferromagnetic di-μ_2-oxo bridged Mn–Mn interactions (2.7—2.75 Å) and a possibly weak-coupling μ_2-oxo bridged one (3.3 Å, bented) are illustrated in Scheme 4. It should be noted that these types of Mn clusters are acceptable only under the limited experimental conditions imposed in this paper. If the simulation of the multiline signal is added to the constraints, these clusters may also be largely ruled out, as indicated by preliminary calculations[58] and a very recent article.[60] This indicates that the magnetic properties of the S_2-state Mn cluster, which exhibits the $g = 2$ multiline EPR signal, may not be explained in terms of any simple-minded modeling work using two or three di-μ_2-oxo bridged Mn–Mn bonds alone, because in Fig. 2 all of the examples of di-μ_2-oxo bridges with 2.65—2.75 Å distances are strong-antiferromagnetic.

Based on these considerations, we suggest that at least one of the observed "2.7 Å" Mn–Mn bonds must be bridged by more sophisticated bridge ligands, such as exemplified in Scheme 1 *b*—*f*, which can be accommodated to both conditions of the 2.7—2.8 Å Mn–Mn distance and a weak-to-intermediate exchange interaction. By this modification, not only Berkeley's model, but also all of the models in Scheme 3, could survive as possible candidates for the S_2-

state Mn cluster. A more significant consequence is that a "distorted cubane" model, as shown in Scheme 5, which must necessarily contain two μ_2-oxo-μ_3-oxo bridged Mn–Mn bonds and at least one μ_2-oxo bridged one to form a triangular Mn_3O_3 core, appears as the most favorable model. This model is involved in all of the maps in Fig. 3, except for Fig. 3C a ($S^* = 1/2$), because at least one μ_2-oxo-μ_3-oxo bridged Mn–Mn bond, which can be equivalently assigned to any one of J_{ai} (i = c, d) and J_{bj} (j = c, d), may be assumed to take an intermediate or strong exchange coupling in the range 40 $cm^{-1} < J_{ac}$ (or J_{bc}). It should be reminded that this trimer-plus-monomer type of distorted cubane model was already proposed.[59] In this model, a somewhat elongated μ_2-oxo-μ_3-oxo bridged Mn(III)–Mn(IV) bond is supposed to be shortened by the presence of a third μ_2-(aqua, hydroxo) or μ_2-carboxylato bridge to yield the observed 2.7 Å Mn–Mn distance.

We can summarize these results as follows:

(1) Although one of the observed "2.7 Å Mn–Mn bonds in the cluster can be reasonably assigned to a strong-antiferromagnetic Mn(III)–Mn(IV) interaction, its bridge ligand may not necessarily be di-μ_2-oxo, as widely accepted, but may be more complicated, as long as the 2.7 Å distance is maintained (see Scheme 1).

(2) The other "2.7 Å" Mn–Mn bond in the normal Mn cluster would really have a slightly longer distance (2.75—2.8 Å) than 2.7 Å, so that the spin-exchange interaction between these Mn ions might show weak or intermediate coupling, similar to the case of the NH_3-treated Mn cluster.

(3) The magnetic data on the ground state and the first excited state (Fig. 1b) could not be explained by four types of Mn clusters, as depicted in Scheme 3, i.e. a tetramer consisting of di-μ_2-oxo bridged Mn(III)–Mn(IV) and Mn(v)–Mn(v) (v = III, IV) dimers (*a* and *b*), a tetramer consisting of a di-μ_2-oxo bridged Mn(III)–Mn(IV) dimer and a strong-antiferromagnetic μ_2-oxo bridged Mn–Mn dimer (*c* and *d*), a propeller-type tetramer in which the central Mn ion is chelated by three di-μ_2-oxo bridged Mn cores (*e* and *f*), and a chain-type tetramer with a linear arrangement of three di-μ_2-oxo bridged Mn–Mn bonds (*g*). These rejectable Mn clusters are exactly defined by the non-shaded regions in the contour maps, *a* and *d*—*f*, in Figs. 3A and B.

(4) Berkeley's model can not be ruled out by the present magnetic data alone (Fig. 1b). It can survive when the second di-μ_2-oxo bridge is replaced by a slightly longer μ_2-oxo-μ_2-hydroxo bridge or a more complicated one, so that the spin-exchange interaction between them might be significantly reduced.

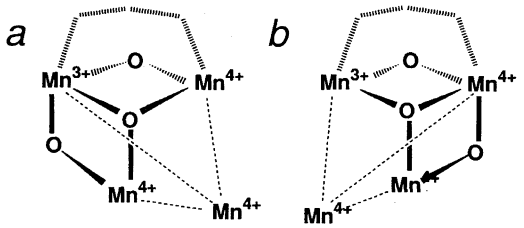

Scheme 5. The most favorable model for the S_2-state Mn cluster, called "a trimer-plus-monomer type of distorted cubane," which is consistent with the magnetic properties, the EXAFS data and the manganese chemistry. About the third bridge ligand denoted by dotted line, see Scheme 1.

(5) A trimer-plus-monomer type of distorted cubane model in Scheme 5, which is involved in all of the maps in Fig. 3, except for Fig. 3C *a*, were found to be most favorable (the total probability is largest). The triangular Mn_3O_3-core in this model is assumed to contain such a third bridge ligand between the μ_2-oxo-μ_3-oxo bridged Mn_a–Mn_b bond, that can shorten the bond length down to '2.7 Å' to satisfy the EXAFS data.

This work was supported by a grant for Photosynthetic Science and a Junior Research Associate Program at RIKEN given by the Science and Technology Agency of Japan, and by Grants-in-Aid for Science Research on Priority Area (No. 09235237 to T.O. and No. 10179219 to M.K.) and by a Grant-in-Aid for Scientific Research (No. 09640783 to T.O.) from the Ministry of Education, Science and Culture. T.O. is indebted for a Special Grant for Promotion of Research from RIKEN.

Appendix

The matrix elements of the spin-exchange hamiltonian (H_{ex}) in the $|(S_{ab})(S_{abc})S>$ and $|(S_{ab})(S_{cd})S>$ coupling schemes are analytically expressed as

$$< S_a S_b (S'_{ab}) S_c (S'_{abc}) S_d SM | H_{ex} | S_a S_b (S_{ab}) S_c (S_{abc}) S_d SM > =$$

$$\frac{J_{ab}}{2}[S_{ab}(S_{ab}+1) - S_a(S_a+1) - S_b(S_b+1)]\delta_{S'_{ab},S_{ab}}\delta_{S'_{abc},S_{abc}}$$

$$+\left[\begin{array}{l} J_{ac}(-1)^{S_a+S_b+S_c+2S_{ab}+S_{abc}+1}\sqrt{S_a(S_a+1)(2S_a+1)} \begin{Bmatrix} S_b & S_a & S'_{ab} \\ 1 & S_{ab} & S_a \end{Bmatrix} \\ +J_{bc}(-1)^{S_a+S_b+S_c+S_{ab}+S'_{ab}+S_{abc}+1}\sqrt{S_b(S_b+1)(2S_b+1)} \begin{Bmatrix} S_a & S_b & S'_{ab} \\ 1 & S_{ab} & S_b \end{Bmatrix} \end{array}\right] \times A_1$$

$$+\left[\begin{array}{l} J_{ad}(-1)^{S'_{ab}+S_{ab}+2S_{abc}}\sqrt{S_a(S_a+1)(2S_a+1)} \begin{Bmatrix} S_b & S_a & S'_{ab} \\ 1 & S_{ab} & S_a \end{Bmatrix} \\ +J_{bd}(-1)^{2S'_{ab}+2S_{abc}}\sqrt{S_b(S_b+1)(2S_b+1)} \begin{Bmatrix} S_a & S_b & S'_{ab} \\ 1 & S_{ab} & S_b \end{Bmatrix} \end{array}\right] \times A_2$$

$$+J_{cd}(-1)^{S_c+S_d+S_{ab}+S'_{abc}+S_{abc}+S+1} \begin{Bmatrix} S & S_d & S'_{abc} \\ 1 & S_{abc} & S_d \end{Bmatrix} \begin{Bmatrix} S_{ab} & S_c & S'_{abc} \\ 1 & S_{abc} & S_c \end{Bmatrix} \delta_{S'_{ab},S_{ab}}$$

$$\times\sqrt{S_c(S_c+1)(2S_c+1)S_d(S_d+1)(2S_d+1)(2S'_{abc}+1)(2S_{abc}+1)}$$

$$A_1 = \sqrt{S_c(S_c+1)(2S_c+1)(2S'_{ab}+1)(2S_{ab}+1)} \begin{Bmatrix} S_{abc} & S_c & S'_{ab} \\ 1 & S_{ab} & S_c \end{Bmatrix} \delta_{S'_{abc},S_{abc}}$$

$$A_2 = (-1)^{S_a+S_b+S_c+S_d+S} \begin{Bmatrix} S & S_d & S'_{abc} \\ 1 & S_{abc} & S_d \end{Bmatrix} \begin{Bmatrix} S_c & S_{ab} & S'_{abc} \\ 1 & S_{abc} & S_{ab} \end{Bmatrix} \times \sqrt{S_d(S_d+1)(2S_d+1)(2S'_{ab}+1)(2S_{ab}+1)(2S'_{abc}+1)(2S_{abc}+1)}, \quad \text{(A1)}$$

and

$$< S_a S_b(S'_{ab}) S_c S_d(S'_{cd}) SM | H_{ex} | S_a S_b(S_{ab}) S_c S_d(S_{cd}) SM > =$$

$$\frac{J_{ab}}{2}[S_{ab}(S_{ab}+1) - S_a(S_a+1) - S_b(S_b+1)]\delta_{S'_{ab},S_{ab}}\delta_{S'_{cd},S_{cd}}$$

$$+ \left[\begin{array}{l} J_{ac}(-1)^{S_{ab}-S'_{ab}}\sqrt{S_c(S_c+1)(2S_c+1)} \begin{Bmatrix} S_d & S_c & S'_{cd} \\ 1 & S_{cd} & S_c \end{Bmatrix} \\ +J_{ad}(-1)^{S_{ab}-S'_{ab}+S'_{cd}-S_{cd}}\sqrt{S_d(S_d+1)(2S_d+1)} \begin{Bmatrix} S_c & S_d & S'_{cd} \\ 1 & S_{cd} & S_d \end{Bmatrix} \end{array} \right]$$

$$\times \sqrt{S_a(S_a+1)(2S_a+1)} \begin{Bmatrix} S_b & S_a & S'_{ab} \\ 1 & S_{ab} & S_a \end{Bmatrix} B$$

$$+ \left[\begin{array}{l} J_{bc}\sqrt{S_c(S_c+1)(2S_c+1)} \begin{Bmatrix} S_d & S_c & S'_{cd} \\ 1 & S_{cd} & S_d \end{Bmatrix} \\ +J_{bd}(-1)^{S'_{cd}-S_{cd}}\sqrt{S_a(S_a+1)(2S_a+1)} \begin{Bmatrix} S_c & S_d & S'_{cd} \\ 1 & S_{cd} & S_d \end{Bmatrix} \end{array} \right]$$

$$\times \sqrt{S_b(S_b+1)(2S_b+1)} \begin{Bmatrix} S_a & S_b & S'_{ab} \\ 1 & S_{ab} & S_b \end{Bmatrix} B$$

$$+\frac{J_{cd}}{2}[S_{cd}(S_{cd}+1) - S_c(S_c+1) - S_d(S_d+1)]\delta_{S'_{ab},S_{ab}}\delta_{S'_{cd},S_{cd}}$$

$$B = (-1)^{S_a+S_b+S_c+S_d+S_{ab}+S'_{ab}+S_{cd}+S'_{cd}+S} \times \sqrt{(2S_{ab}+1)(2S'_{ab}+1)(2S_{cd}+1)(2S'_{cd}+1)} \begin{Bmatrix} S & S'_{ab} & S'_{cd} \\ 1 & S_{cd} & S_{ab} \end{Bmatrix}, \quad \text{(A2)}$$

where the algebraic expressions of the Wigner 6-j symbols are given in Table 9.2,[49] and $\begin{Bmatrix} a & b & c \\ 1 & c' & b \end{Bmatrix}$ can take non-zero values only for $c'-c = 0, \pm 1$. [Note: Bencini & Gatteschi[52] gave only the matrix elements of $\boldsymbol{S_a}\cdot\boldsymbol{S_b}$, $\boldsymbol{S_b}\cdot\boldsymbol{S_c}$, and $\boldsymbol{S_c}\cdot\boldsymbol{S_d}$ in the $|(S_{ab})(S_{abc})S>$ scheme but did neither of $\boldsymbol{S_a}\cdot\boldsymbol{S_c}$ in this scheme nor any in the $|(S_{ab})(S_{cd})S>$ scheme. Moreover, a matrix element in Eq. (4.39), $< S_1S_2S_{12}S_3S_{123}S_4SM|\boldsymbol{S_2}\cdot\boldsymbol{S_3}|S_1S_2S'_{12}S_3S'_{123}S_4SM>$, involves an incorrect phase factor, $(-1)^{S'_{12}+S_{12}+S_1+S_2+S_3+S+1}$, which should be corrected into $(-1)^{S'_{12}+S_{12}+S_1+S_2+S_3+S_{123}+1}$ (in our notation, 1→a, 2→b, 3→c and 4→d). On the other hand, Belinskii gave only the matrix elements of H_{ex} in the $|(S_{ab})(S_{cd})S>$ scheme.[30] But, the presented non-diagonal matrix elements are specified for the case of $S_a = S_b$ and are not general. Moreover, the reported diagonal matrix elements contain two misprints or errors: i.e., in Eq. (23), the terms, $-J_{12}S_{12}(S_{12}+1)-J_{34}[S_{34}(S_{34}+1)-3/4]$, should be replaced by $-J_{12}[S_{12}(S_{12}+1)-S_1(S_1+1)-S_2(S_2+1)]-J_{34}[S_{34}(S_{34}+1)-S_3(S_3+1)-S_4(S_4+1)]$ (in our notation, $J_{12} \rightarrow -J_{ab}/2$ and $J_{34} \rightarrow -J_{cd}/2$)].

References

1) R. J. Debus, *Biochim. Biophys. Acta*, **1102**, 269 (1992).

2) R. D. Britt, in "Oxygenic Photosynthesis: The Light Reactions," ed by D. R. Ort and C. F. Yocum, Kluwer Academic Publishers, Dordrecht (1996), p. 137.

3) V. K. Yachandra, S. Sauer, and M. P. Klein, *Chem. Rev.*, **96**, 2927 (1996).

4) W. Rüttinger and G. C. Dismukes, *Chem. Rev.*, **97**, 1 (1997).

5) P. Joliot, G. Barbieri, and R. Chabaud, *Photochem. Photobiol.*, **10**, 309 (1969).

6) B. Kok, B. Fourbush, and M. McGloin, *Photobiol.*, **11**, 457 (1970).

7) T.-A. Ono, T. Noguchi, Y. Inoue, M. Kusunoki, T. Matsushita, and H. Oyanagi, *Science*, **258**, 1335 (1992).

8) M. Kusunoki, T. Ono, T. Noguchi, Y. Inoue, and H. Oyanagi, *Photosynth. Res.*, **38**, 331 (1993).

9) M. Kusunoki, T. Ono, M. Suzuki, T. Noguchi, A. Uehara, T. Matsushita, H. Oyanagi, and Y. Inoue, in "Synchrotron Radiation in the Biosciences," ed by B. Chance, et al., Oxford Science Publications, Oxford (1994), p. 284.

10) T. A. Roelofs, W. Liang, J. J. Latimer, R. M. Ginco, A. Ronpel, J. C. Andrews, K. Sauer, K. Yachandra, and M. P. Klein, *Proc. Natl. Acad. Sci. U.S.A.*, **93**, 3335 (1996).

11) A.-F. Miller and G. W. Brudvig, *Biochim. Biophys. Acta*, **1056**, 1 (1991).

12) T. Vänngård, Ö. Hanson, and A. Haddy, in "Manganese Redox Enzymes," ed by V. L. Pecoraro, VCH Publishers, New York (1992), p. 105.

13) G. C. Dismukes and Y. Siderer, *Proc. Natl. Acad. Sci. U.S.A.*, **78**, 274 (1981).

14) K. A. Åhrling and R. J. Pace, *Biophys. J.*, **68**, 2081 (1995).

15) J. Bonvoisin, G. Blondin, J.-J. Girerd, and J.-L. Zimmermann, *Biophys. J.*, **61**, 1076 (1992).

16) M. Zheng and G. C. Dismukes, *Inorg. Chem.*, **35**, 3307 (1996).

17) M. Kusunoki, *Chem. Phys. Lett.*, **197**, 108 (1992).

18) K. Hasegawa, M. Kusunoki, Y. Inoue, and T. Ono, *Biochemistry*, **37**, 9457 (1998).

19) Ö. Hansson, R. Aasa, and T. Vänngård, *Biophys. J.*, **51**, 825 (1987).

20) R. J. Pace, P. Smith, R. Bramley, and D. Stehlik, *Biochim. Biophys. Acta*, **1058**, 161 (1991).

21) G. A. Lorigan and R. D. Britt, *Biochemistry*, **33**, 12072 (1994).

22) G. C. Dismukes, K. Ferris, and P. Watnick, *Photobiochim. Photobiophys.*, **3**, 243 (1982).

23) M. Kusunoki, in "Research in Photosynthesis," ed by N. Murata, Kluwer Academic Publishers, Dordrecht (1995), Vol. II, p. 297.

24) G. N. George, R. C. Prince, and S. P. Cramer, *Science*, **242**, 789 (1989).

25) J. E. Penner-Hahn, R. M. Fronko, V. L. Pecoraro, C. F. Yocum, S. D. Betts, and N. R. Bowlby, *J. Am. Chem. Soc.*, **112**, 2549 (1990).

26) V. J. DeRose, I. Mukerji, M. J. Latimer, V. K. Yachandra, K. Sauer, and M. P. Klein, *J. Am. Chem. Soc.*, **116**, 5239 (1992).

27) D. J. MacLachlan, B. J. Hallahan, S. V. Ruffle, J. H. A. Nugent, M. C. W. Evans, R. W. Strange, and S. S. Hasnain, *Biochem. J.*, **285**, 569 (1992).

28) V. K. Yachandra, V. J. DeRose, M. J. Latimer, I. Mukerji, K. Sauer, and M. P. Klein, *Science*, **260**, 675 (1993).

29) M. Kusunoki, T. Takano, T. Ono, T. Noguchi, Y. Yamaguchi, H. Oyanagi, and Y. Inoue, in "Photosynthesis: from Light to Biosphere," ed by P. Mathis, Kluwer Academic Publishers, Dordrecht (1995), Vol. II, p. 251.

30) M. I. Belinskii, *Chem. Phys.*, **179**, 1 (1994).

31) J. Máthá, C. J. Schinkel, and W. A. Van Amstel, *Chem. Phys.*

Lett., **33**, 528 (1975).
32) D. V. Behere, V. R. Marathe, and S. Mitra, *Chem. Phys. Lett.*, **81**, 57 (1981).
33) B. J. Kennedy and K. S. Murray, *Inorg. Chem.*, **24**, 1552 (1985).
34) H. Kawasaki, M. Kusunoki, Y. Hayashi, M. Suzuki, K. Munezawa, M. Suenaga, H. Senda, and A. Uehara, *Bull. Chem. Soc. Jpn.*, **67**, 1310 (1994).
35) S. K. Chandra and A. Chakravorty, *Inorg. Chem.*, **31**, 760 (1992).
36) D. A. Varshalovich, A. N. Moskalev, and V. K. Khersonskii, "Quantum Theory of Angular Momentum," World Scientific, Singapore (1988).
37) A. R. Edmonds, "Angular Momentum in Quantum Mechanics," Princeton University Press, New York (1960).
38) J. S. Griffith, *Molec. Phys.*, **24**, 833 (1972).
39) A. Bencini and D. Gatteschi, "EPR of Exchange Coupled Systems," Springer-Verlag, Berlin (1990), p. 86.
40) H. Dau, J. C. Andrews, T. A. Roelof, M. J. Latimer, W. Liang, V. K. Yachandra, K. Sauer, and M. P. Klein, *Biochemistry*, **34**, 5274 (1995).
41) M. Stebler, A. Ludi, and H.-B. Bürgi, *Inorg. Chem.*, **25**, 4743 (1986).
42) G. Cristou, *Acc. Chem. Res.*, **22**, 328 (1989).
43) K. Wieghart, *Angew. Chem., Int. Ed. Engl.*, **28**, 1153 (1989).
44) C. A. Kipke, M. J. Scott, J. W. Gohdes, and W. H. Armstrong, *Inorg. Chem.*, **29**, 2193 (1990).
45) P. A. Goodson, A. R. Oki, J. Glerup, and D. J. Hodgson, *J. Am. Chem. Soc.*, **112**, 6248 (1990).
46) S. Pal, M. K. Chan, and W. H. Armstrong, *J. Am. Chem. Soc.*, **114**, 6398 (1992).
47) R. Manchanda, G. W. Brudvig, and R. H. Crabtree, *Coord. Chem. Rew.*, **144**, 1 (1995).
48) A. Magnuson and S. Styring, private communication.
49) D. Koulougliotis, R. H. Schweitzer, and G. W. Brudvig, *Biochemistry*, **36**, 9735 (1997).
50) J. W. Gohdes and W. H. Armstrong, *Inorg. Chem.*, **31**, 368 (1992).
51) M. Rapta, P. Kamaras, G. A. Brewer, and G. B. Jameson, *J. Am. Chem. Soc.*, **117**, 12865 (1995).
52) J. E. Sarneski, M. Didiuk, H. H. Thorp, R. H. Crabtree, G. W. Brudvig, J. W. Faller, and G. K. Schulte, *Inorg. Chem.*, **30**, 2833 (1991).
53) K. Hasegawa, Ph. M. Thesis, Meiji University, Japan (1995).
54) J. H. Wilkinson and C. Reinsch, "Handbook for Automatic Computation," Springer-Verlag, New York (1971), Vol. II.
55) K. Sauer, V. K. Yachandra, R. D. Britt, and M. P. Klein, in "Manganese Redox Enzymes," ed by V.L. Pecoraro, VCH Publishers, New York (1992), p. 141.
56) T. Takano and M. Kusunoki, submitted for publication.
57) W. Liang, M. J. Latimer, H. Dau, T. A. Roelofs, V. K. Yachandra, K. Sauer, and M. P. Klein, *Biochemistry*, **33**, 4923 (1994).
58) K. Hasegawa and M. Kusunoki, in "Photosynthesis: from Light to Biosphere," ed by P. Mathis, Kluwer Academic Publishers, Dordrecht (1995), Vol. II, p. 341.
59) M. Kusunoki, *Chem. Phys. Lett.*, **239**, 148 (1995).
60) H. Hasegawa, T. Ono, Y. Inoue, and K. Kusunoki, *Chem. Phys. Lett.*, **300**, 9 (1999).